# On Detection of a Global Mode Structure in Experiments by Use of Turbulence Diagnostic Simulator

Naohiro KASUYA, Seiya NISHIMURA, Masatoshi YAGI[1,2], Kimitaka ITOH and Sanae-I ITOH[1]

*National Institute for Fusion Science, 322-6 Oroshi-cho, Toki, Gifu 509-5292, Japan*
[1]*Research Institute for Applied Mechanics, Kyushu University, 6-1 Kasuga-kouen, Kasuga, Fukuoka 816-8580, Japan*
[2]*Japan Atomic Energy Agency, 801-1 Mukoyama, Naka, Ibaraki 311-0193, Japan*

(Received 27 July 2010 / Accepted 18 November 2010)

Development of experimental diagnostics in fusion plasmas has made possible to measure plasma fluctuations with high spatial and temporal resolution. To detect a global mode, which contributes to global transport phenomena, it is helpful to use simulation data as a test field for the measurements. The turbulence diagnostic simulator is an assembly of codes for turbulence simulations and numerical diagnostics. Using the turbulence diagnostic simulator, a time series of turbulence data is obtained, on which numerical diagnostics are carried out to demonstrate how global modes to be observed. There exist modes, which are broad in the radial direction, and correlation analyses reveal the characteristic structures with a finite number of local observations in the radial direction, as in experiments.



Keywords: turbulence simulation, structural formation, numerical diagnostic, fluctuation measurement, non-local transport

DOI: 10.1585/pfr.6.1403002

## 1. Introduction

Turbulent plasmas form a variety of nonlinear structures [1, 2]. A global structure, which spreads broadly in the radial direction, can be excited. A local change of the plasma state contributes to the whole of the structure immediately, so the global structure is one of the candidates for contributor to the non-local transport [3, 4]. Therefore, it is important to detect the global structure and clarify its role on the transport.

Development of experimental diagnostics in fusion plasmas has made possible to measure plasma fluctuations with high spatial and temporal resolution [5, 6], and spectral analyses of the data reveal the turbulent structure in linear devices [7–9] and toroidal devices [10–13]. Usually a limited number of lines of sight can be used for measurements in experiments, so the information of a three-dimensional (3-D) structure is limited. Therefore, it is helpful to use time series of 3-D simulation data as a test field for the measurements [14]. We have been developing a turbulence diagnostic simulator, which simulates turbulence diagnostics numerically. Data analyses as same in the experiments are carried out on the simulation data of plasma turbulence [15].

In this article, we demonstrate the detection of global mode structures with a finite number of local observations on 3-D numerical simulation data of plasma turbulence. A reduced MHD model is used for generation of turbulent fields in a helical plasma, and numerical diagnostics are carried out on the time series of the 3-D turbulent data. A global mode is identified from the data including various modes. An example of the time evolution of a mode, which is broad in the radial direction, is obtained by subtracting a single mode from those included in turbulence simulation, and the characteristic structure of the mode is revealed from the local observations on the data.

*author's e-mail: kasuya@nifs.ac.jp*

## 2. Generation of Turbulent Fields

To provide turbulence data, the simulation code of the resistive drift wave turbulence in a linear device, called 'Numerical Linear Device' [16] has been extended to calculate the drift-interchange turbulence in helical plasmas with a circular cross-section. The averaging method with the stellarator expansion [17, 18] is applied to give a set of model equations as

$$\frac{\partial \nabla_\perp^2 u}{\partial t} = [u, \nabla_\perp^2 u] + \nabla_{/\!/} \nabla_\perp^2 A + [\Omega, P] + \mu \nabla_\perp^4 u, \quad (1)$$

$$\frac{\partial A}{\partial t} = \nabla_{/\!/}(u + \alpha P) + \eta \nabla_\perp^2 A, \quad (2)$$

$$\frac{\partial P}{\partial t} = [u, P] - C \nabla_{/\!/} \nabla_\perp^2 A + \eta_\perp \nabla_\perp^2 P + S, \quad (3)$$

where $u$ is the stream function, $A$ is the $\zeta$ component of the vector potential, $P$ is the total pressure, $\nabla_{/\!/} = \partial/\partial\overline{\zeta} + [\ \ , \Psi]$, $\Psi = A - (1/2)\overline{\nabla\langle\Phi\rangle \times \nabla\Phi}\hat{\zeta}$, $\Phi$ is the magnetic potential, $\alpha = V_\mathrm{A}/(2\Omega_\mathrm{ci}a)$, $C = \gamma P_0 V_\mathrm{A}/(\Omega_\mathrm{ci}a)$, $\Omega = 2r\cos\theta + \overline{(\nabla\Phi)^2}$ is the magnetic curvature, $S$ is the pressure source, $V_\mathrm{A}$ is the Alfvén velocity, $\Omega_\mathrm{ci}$ is the ion cyclotron frequency, $a$ is the minor radius, $\gamma$ is the specific heat ratio, $\eta$ is the resistivity, $\mu$ and $\eta_\perp$ are viscosities, $\overline{f}$

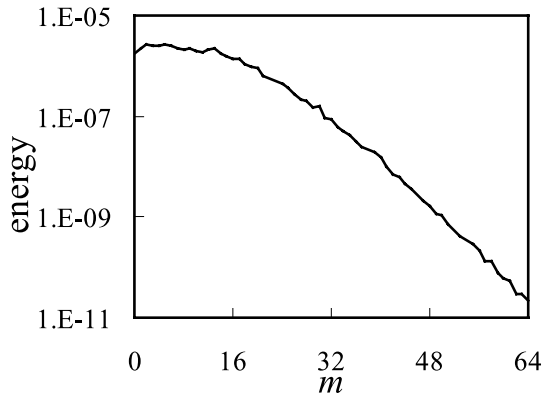


Fig. 1 Potential energy spectrum on poloidal mode number $m$ in the nonlinear saturation state.

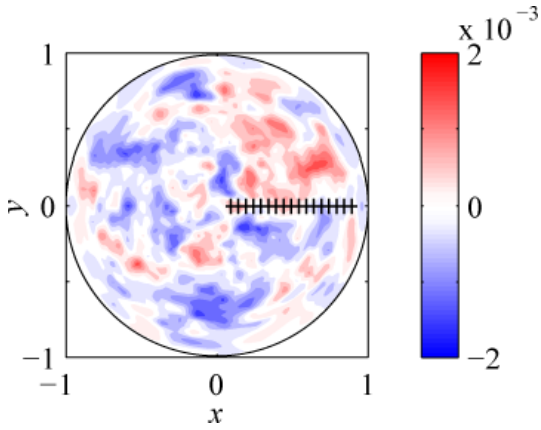


Fig. 2 Snapshot of the contours of the electrostatic potential. The poloidal cross-section at $\zeta = 0$ and $t = 3000$ is shown, where the plane with $y = 0$ is the midplane, the region with $x > 0$ is the low field side, and $(x, y)$ is the Cartesian coordinates whose origin is set at the center of the plasma. Locations where local observations are carried out are indicated by 17 crosses (+) in this figure.

is the average of $f$ over the helical pitch length, and [ ] is the Poisson bracket. The following normalizations are used in the model equations: $u/(\varepsilon a V_{\rm A}) \to u, A/(\varepsilon a B_0) \to A, P/(\varepsilon B_0^2/\mu_0) \to P, t/t_{\rm A} \to t$, and $r/a \to a$, where $\varepsilon$ is the inverse aspect ration and $t_{\rm A} = a/(\varepsilon V_{\rm A})$ is the Alfvén time. Here, we assume that variable $u$ represents the normalized electrostatic potential.

Equations (1) - (3) are solved in the toroidal coordinates with spectral expansion in the poloidal and toroidal directions. The boundary conditions in the radial direction are set to $f = 0$ at $r = 0$, 1 when $m \neq 0$, and $\partial f/\partial r = 0$ at $r = 0$, $f = 0$ at $r = 1$ when $m = 0$, where $f$ implies $\{u, A, P\}$, $m$ is the poloidal mode number, and $r = 1$ gives an outer boundary of the plasma. In the initial state the pressure profile is given to be flat. The pressure source is fixed to be

$$S(r) = \frac{4S_0\mu_{\rm N}}{L_{\rm N}}\left[1 - \left(\frac{r}{L_{\rm N}}\right)^2\right]\exp\left[-\left(\frac{r}{L_{\rm N}}\right)^2\right], \qquad (4)$$

with $S_0 = 0.2$, $L_{\rm N} = 0.6\,{\rm m}$, which forms the profile peaked at $r = 0$. The magnetic potential is given by

$$\Phi = 2\Phi_l I_l(hr)\sin(l\theta + h\zeta), \qquad (5)$$

where $I_l$ is the modified Bessel function, $l$ is the pole number of the helical winding, $h = M/R_0$, $M$ is the pitch number, $R_0$ is the major radius, and $\Phi_l$ is a constant coefficient. The following parameters are used: $B = 2.0\,{\rm T}$, $T_e = 1\,{\rm keV}$, $a = 0.6\,{\rm m}$, $R_0 = 3.75\,{\rm m}$, $\mu = \eta = \eta_\perp = 1 \times 10^{-5}$, $l = 2$, $M = 10$, $\Phi_l = 0.2$. Rotational transform $\iota$ is give by a monotonically increasing function with the radius from $\iota(0) = 0.41$ to $\iota(1) = 1.17$.

Simulations are performed with 1024 grids in the radial direction. Fourier modes $-64 \le m \le 64$, $-16 \le n \le 16$ are taken, where $n$ is the toroidal mode number. Spatio-temporal data of turbulent fields are generated by this global simulation. Low $m$, $n$ modes are excited in the linear growing phase, and saturation is obtained with energy exchange between various modes by nonlinear couplings. Figure 1 shows the energy spectrum of the electrostatic potential on $m$ in the nonlinear saturation state. These excited modes give the electrostatic potential profile as in Fig. 2.

# 3. Numerical Diagnostic on Simulation Data

## 3.1 Set up of a one-dimensional array of diagnostics

In experiments, a finite number of local observations give the radial profile. Here we carry out the analysis simulating the experimental measurement on the time series of 3-D fields calculated in Sec. 2. One-dimensional (1-D) signals at $\theta = 0$ and $\zeta = 0$ are taken from 3-D fields to show the radial profile. Data on 17 points, shown by crosses on Fig. 2, give the time evolution of the radial profile of the electrostatic potential as in Fig. 3 (a). The electrostatic potential oscillates in the whole region of the plasma. Figure 3 (c) shows the frequency spectrum at $r = 0.4a$, calculated from the time series data shown in Fig. 3 (b). Coherent modes exist near $f \sim 0.025$, 0.051, 0.076 and so on. There are global modes with poloidal mode number $m = 0$ in these frequency ranges, which give the sharp peaks in the spectrum.

## 3.2 Spatio-temporal correlation

The time evolution of the radial profile as in Fig. 3 (a) suggests the existence of a global mode. However, its envelope is modulated from time to time, so the relation between different radial positions of the plasma is not clear. We discuss the process for the deduction of the structure in this subsection. A correlation analysis is carried out to find out the characteristic structure. Here the data set from

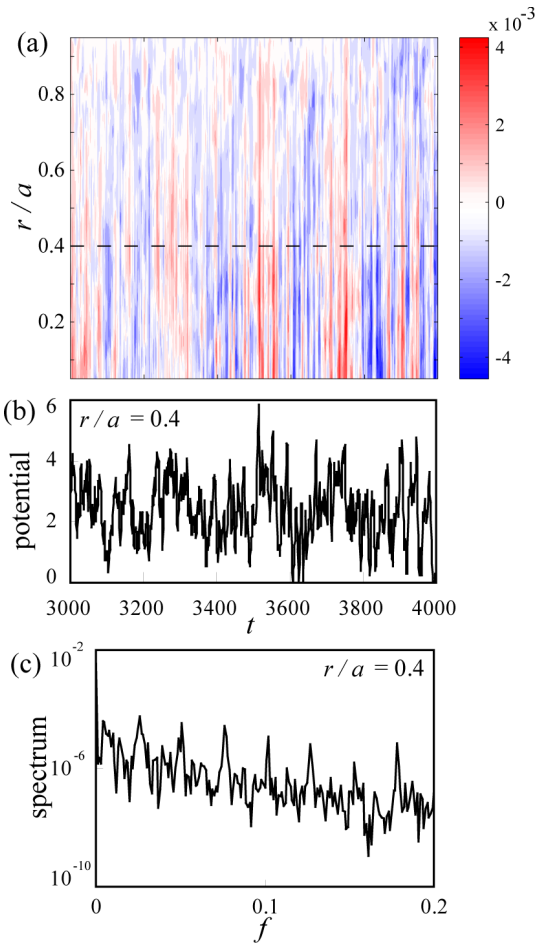


Fig. 3 (a) Time evolution of the radial profile of the electrostatic potential at $\theta = 0$ and $\zeta = 0$. (b) Time evolution of the electrostatic potential at $r = 0.4a$, indicated by the dashed line in (a). (c) Frequency spectrum of (b).

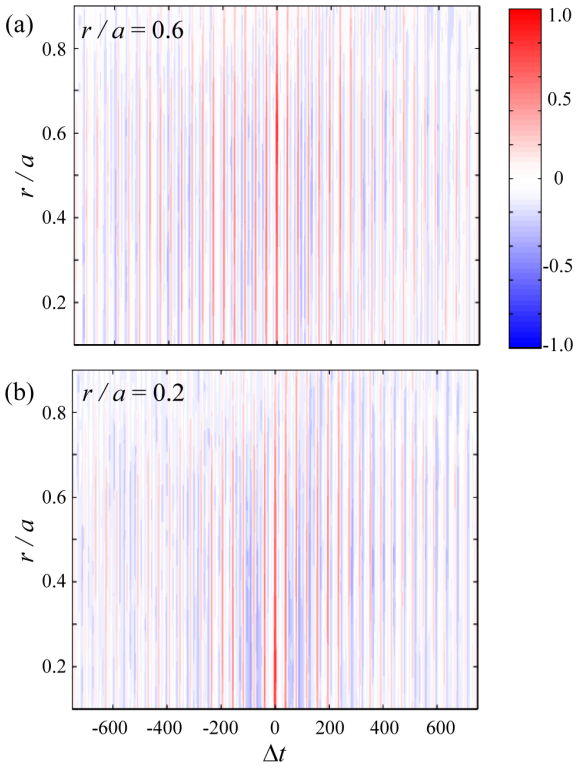


Fig. 4 Cross-correlation functions between different radial positions. The reference positions are set at $r =$ (a) $0.6a$ and (b) $0.2a$.

$t = 3000t_A$ to $5000t_A$ is analyzed, which corresponds to the duration of about $30(a/c_s)$, where $c_s$ is the ion sound velocity. Figures 4 show the cross-correlation functions between different radial positions. Two reference points are selected at $r = 0.2a$ and $0.6a$. At the both points, the oscillation corresponding to the fundamental frequency in Fig. 3 (c) is sustained for a long duration, and there are large correlations with the whole of the other radial position. In this way, existence of the global mode is clearly shown by this correlation analysis with the 1-D set of fluctuation signals.

# 4. Identification of Radial Structures

## 4.1 Target fluctuations

Global structures of fluctuations have been studied with the turbulence data in the previous section. In this section, a single mode $(m, n) = (1, 2)$ is artificially subtracted from the various modes excited in the nonlinear simulation. The subtracted mode is not dominant, and the rational surface with $\iota = 2/1$ does not exist inside the plasma in this simulation. The snapshot of the contours and eigen-

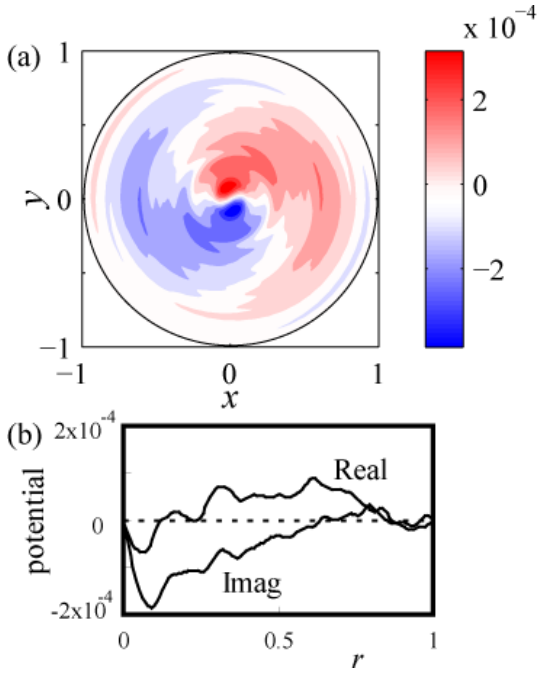


Fig. 5 Snapshot of (a) the contours and (b) eigenfunction of the (1, 2) mode at $t = 3000$.

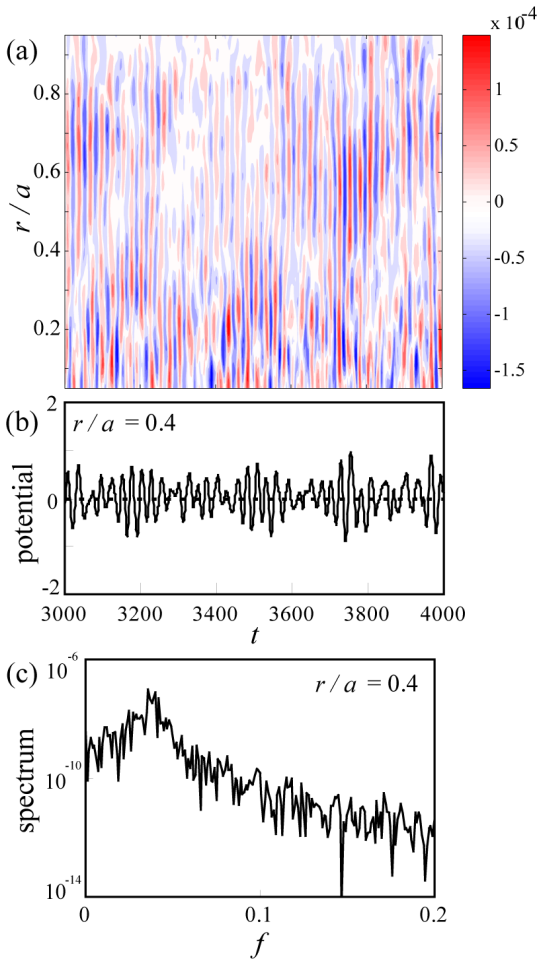


Fig. 6 (a) Time evolution of the radial profile of the electrostatic potential of the (1, 2) mode at $\theta = 0$ and $\zeta = 0$. (b) Time evolution of the electrostatic potential at $r = 0.4a$. (c) Frequency spectrum of (b).

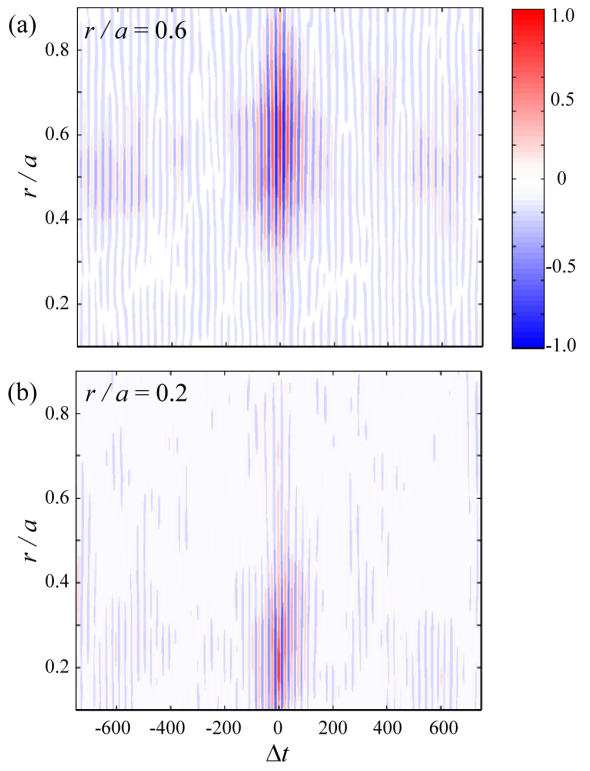


Fig. 7 Cross-correlation functions of the (1, 2) mode between different radial positions. The reference positions are set at $r$ = (a) $0.6a$ and (b) $0.2a$.

function of the (1, 2) mode are shown in Fig. 5. This mode is selected as an example of a mode with a radial structure and transient evolution, and estimation of its structure is demonstrated.

A finite number of local observations at the same positions with those shown in Fig. 2 give the time evolution of the radial profile of the electrostatic potential as in Fig. 6 (a). The electrostatic potential oscillates in the whole region of the plasma, and its envelope is modulated from time to time. However, the relation between different radial positions of the plasma is not clear from this figure.

## 4.2 Spatio-temporal correlation

Global structures of fluctuations are deduced from signals of the 1-D array. A spectrum analysis is carried out. Figure 6 (c) shows the frequency spectrum at $r = 0.4a$, calculated from the time series data shown in Fig. 6 (b). A peak exists near $f \sim 0.04$. A peak in the same frequency range also exists at different radii.

A correlation analysis gives the feature that the mode structure can be divided into two parts whose boundary is located at $r \sim 0.4a$. Figures 7 show the cross-correlation functions between different radial positions. Two reference points are selected at $r = 0.2a$ and $0.6a$. The half width at half maximum (HWHM) of the envelope is evaluated as a typical sustaining duration of the structure. Temporal sustaining durations HWHM are $27t_A$ and $68t_A$ at $r = 0.2a$ and $0.6a$, respectively, so the structure is sustained longer in the outer region. The spatial correlation lengths HWHM are $0.10a$ and $0.21a$ at $r = 0.2a$ and $0.6a$, respectively. The result shows that the structures at $r = 0.2a$ and $0.6a$ are not strongly connected with each other, and there are two structures; one exists in the inner part of the plasma around the position at $r = 0.2a$, and the other exists in outer region around $r = 0.6a$. There is overlap of them in the intermediate region around $r = 0.4a$.

Transient evolution can also be studied by this correlation method. The structure at $r = 0.4a$ is sometimes the part of the inner and sometimes the part of the outer. There is a moment when a large structure appears as shown in Fig. 5, which includes both of the inner and outer structure. The temporal sustaining duration and spatial correlation length is $45t_A$ and $0.27a$, respectively, so the correlation length is the largest at $r = 0.4a$. In this way the spatial and temporal mode structure of the subtracted mode is identified by calculating the radial correlation of fluctuations. The physical mechanism of the structural formation

will be discussed in separated articles.

# 5. Summary

In summary, we have carried out the nonlinear simulation of the drift-interchange turbulence in the helical plasma. Two examples of 1-D data sets were subtracted from the 3-D turbulence data; one including all modes calculated in the nonlinear simulation, and the other including only single mode broad in the radial direction. The analyses on the data show the characteristic radial structures of the dominant mode and the subtracted mode, respectively, and are found to be effective for identification of the global structures. If the number of the detection point is too small to identify the structure in experiments, the analysis gives estimation of the appropriate number of observations. This is preparation of more sophisticated comparison between experiments and numerical simulations of plasma turbulence.

# Acknowledgments

The authors acknowledge discussions with Prof. A. Fujisawa, Prof. K. Ida, Prof. A. Fukuyama, Dr. S. Inagaki, Dr. Y. Nagashima, and Dr. T. Yamada. This work is supported by the Grant-in-Aid for Young Scientists (20760581) and for Scientific Research (19360418, 21224014) of JSPS, by the collaboration program of NIFS (NIFS09KTAD009, NIFS09KDAD009, NIFS10KLHH315) and of RIAM of Kyushu University.

[1] See reviews, e.g. P.H. Diamond, S.-I. Itoh, K. Itoh and T.S. Hahm, Plasma Phys. Control. Fusion **47**, R35 (2005).
[2] A. Yoshizawa, S.-I. Itoh and K. Itoh, *Plasma and Fluid Turbulence* (IOP Publishing, Bristol, 2003).
[3] P.H. Diamond and T.S. Hahm, Phys. Plasmas **2**, 2292 (1995).
[4] S.-I. Itoh and K. Itoh, Plasma Phys. Control. Fusion **43**, 1055 (2001).
[5] A. Fujisawa, Nucl. Fusion **49**, 013001 (2009).
[6] G.R. Tynan, A. Fujisawa and G. McKee, Plasma Phys. Control. Fusion **51**, 113001 (2009).
[7] T. Yamada, S.-I. Itoh, T. Maruta, N. Kasuya, Y. Nagashima, S. Shinohara, K. Terasaka, M. Yagi, S. Inagaki, Y. Kawai, A. Fujisawa and K. Itoh, Nature Phys. **4**, 721 (2008).
[8] G.Y. Antar, J.H. Yu and G. Tynan, Phys. Plasmas **14**, 022301 (2007).
[9] T. Windisch, O. Grulke and T. Klinger, Phys. Plasmas **13**, 122303 (2006).
[10] P.A. Politzer, Phys. Rev. Lett. **84**, 1192 (2000).
[11] G.D. Conway, Plasma Phys. Control. Fusion **50**, 124026 (2008).
[12] T. Ido, A. Shimizu, M. Nishiura, H. Nakano, S. Kato, S. Ohshima, Y. Yoshimura, S. Kubo, T. Shimozuma, H. Igami, H. Takahashi, K. Toi, F. Watanabe, K. Narihara and I. Yamada, Plasma Sci Technol. **11**, 460 (2009).
[13] S. Inagaki, T. Tokuzawa, K. Itoh, K. Ida, S.-I. Itoh, N. Tamura, S. Sakakibara, N. Kasuya, A. Fujisawa, S. Kubo, T. Shimozuma, T. Ido, S. Nishimura, H. Arakawa, T. Kobayashi, K. Tanaka, Y. Nagayama, K. Kawahata, S. Sudo, H. Yamada, A. Komori and LHD Experimental Group, submitted to Phys. Rev. Lett.
[14] N. Kasuya, S. Nishimura, M. Yagi, K. Itoh, S.-I. Itoh and N. Ohyabu, J. Plasma Fusion Res. SERIES **9**, 523 (2010).
[15] S. Nishimura, N. Kasuya, M. Yagi, K. Itoh, S.-I. Itoh and N. Ohyabu, Plasma Fusion Res. **5**, S2057 (2010).
[16] N. Kasuya, M. Yagi, K. Itoh and S.-I. Itoh, Phys. Plasmas **15**, 052302 (2008).
[17] J.M. Green and J.L. Johnson, Phys. Fluids **4**, 875 (1961).
[18] M. Wakatani, *Stellarator and Heliotron Devices* (Oxford University Press, Oxford 1998).